The pH sensitivity of –NH exchange in LnDOTA–tetraamide complexes varies with amide substituent

Ana Christina L. Opina[a], Yunkou Wu[a], Piyu Zhao[a], Garry Kiefer[a,c] and A. Dean Sherry[a,b]*

The amide proton exchange rates in various lanthanide(III) DOTA–tetraamide complexes were investigated by CEST as a function of variable chemical structures and charges on the amide substituents. Comparisons were made between YbDOTA–(gly)$_4^-$ (Yb-1), YbDOTA–(NHCH$_2$PO$_3$)$_4^{5-}$ (Yb-2) and YbDOTA–(NHCH$_2$PO$_3$Et$_2$)$_4^{3+}$ (Yb-3). The general shapes of the CEST vs pH profiles were similar for the three complexes but they showed maximum CEST intensities at different pH values, pH 8.3, 8.8 and 6.9 for Yb-1, Yb-2 and Yb-3, respectively. This indicates that a more negatively charged substituent on the amide helps stabilize the partial positive charge on the amide nitrogen and consequently more base is required to catalyze proton exchange. The chemical shifts of the –NH protons in Yb-1 and Yb-2 were similar (−17 ppm) while the –NH proton in Yb-3 was at −13 ppm. This shows that the crystal field produced by the amide oxygen donor atoms in Yb-3 is substantially weaker than that in the other two complexes. In an effort to expand the useful range of pH values that might be measured using these complexes as CEST agents, the shapes of the CEST vs pH curves were also determined for two thulium(III) complexes with much larger hyperfine shifted –NH proton resonances. The ratio of CEST from –NH exchange in Tm-1 compared with CEST from –NH exchange in Tm-3 was found to be linear over an extended pH range, from 6.3 to 7.4. This demonstrates a potential advantage of using mixtures of lanthanide(III) DOTA–tetraamides for mapping tissue pH by use of ratiometric CEST imaging. Copyright © 2011 John Wiley & Sons, Ltd.

Keywords: MRI; contrast agents; pH-responsive agents; paramagnetic agents; chemical exchange saturation transfer (CEST) agents; amide proton exchange; ratiometric analysis

1. INTRODUCTION

Chemical exchange saturation transfer (CEST), first demonstrated by Wolff and Balaban in 1989, is an image contrast mechanism based on chemical exchange of saturated spins (1,2). CEST contrast is achieved by applying a frequency-selective presaturation pulse at the resonant frequency of a labile solute proton which is then chemically transferred into another pool of spins. In most cases, the second pool corresponds to bulk water protons, so turning on CEST contrast produces a decrease in the bulk water signal intensity and a consequent darkening of an MR image. Numerous endogenous and exogenous diamagnetic CEST agents (DIACEST) have been reported but here the chemical shift differences between the two exchanging pools make selective excitation somewhat problematical (3). One solution to this limitation is to use an exogenous paramagnetic lanthanide complexes containing hyperfine-shifted exchange sites (PARACEST) (4–6) so that selective irradiation can be performed without significant off-resonance saturation of bulk water protons.

One of the most important determinants of CEST is the proton or water molecule exchange rate (k_{ex}). The residence lifetime ($\tau_M = 1/k_{ex}$) is defined as the time a labile proton or molecule remains at one site before it exchanges into the other. τ_M cannot be too short because it becomes difficult to fully saturate a spin pool before exchange occurs nor should it be so long that magnetization returns back to equilibrium via spin-lattice relaxation (T_1) before exchange occurs. These scenarios limit the observable CEST effect.

A second factor is that τ_M must be in the slow-to-intermediate exchange regime defined as:

$$\tau_M * \Delta\omega > 1 \tag{1}$$

where $\Delta\omega$ is the frequency difference between the exchanging protons or water molecules. It has also been shown from basic Bloch theory that the optimal residence lifetime also depends on the power of the pulse (B_1) used to excite the exchanging protons or water molecules (7,8),

$$\tau_M = 1/(2\pi B_1) \tag{2}$$

* Correspondence to: A. Dean Sherry, Advanced Imaging Research Center, UT Southwestern Medical Center, 5323 Harry Hines Blvd, Dallas, TX 75390-8568, USA.
E-mail: dean.sherry@utsouthwestern.edu

a A. C. L. Opina, Y. Wu, P. Zhao, G. Kiefer, A. D. Sherry
Department of Chemistry, University of Texas at Dallas, 800 W. Campbell Road, Richardson, TX 75083-0688, USA

b A. D. Sherry
Advanced Imaging Research Center, UT Southwestern Medical Center, 5323 Harry Hines Blvd, Dallas, TX 75390-8568, USA

c G. Kiefer
Macrocyclics, 1309 Record Crossing, Dallas, TX 75235, USA

This indicates that at low B_1 (maybe limited to 50–100 Hz for clinical applications), the optimal exchange lifetime for CEST can be estimated to be about 1–3 ms. To date, the bound water lifetime in typical Eu(III) complexes is in the 100–400 μs range so further work must be done to slow the rate of water exchange to make it practical.

It has also been shown that the rates of proton exchange between a labile –NH proton and bulk water are relatively slow (ms range) and generally increase with increasing pH (9,10). This makes such exchange sites potentially useful as pH sensors. For example, the four equivalent amide protons of LnDOTA–(gly)$_4^-$ have been previously shown (11,12) to have a pH-sensitive CEST signal in the range of interest for physiological pH measurements. In this work, we explored the effect of modifying the properties of the amide side chains of other LnDOTA–tetraamide complexes on the amide proton lifetimes as determined by CEST. High-resolution NMR and CEST measurements were performed on Yb(III) and Tm(III) complexes of DOTA–(gly)$_4^-$, DOTA–(NHCH$_2$PO$_3$)$_4^{5-}$ and DOTA–(NHCH$_2$PO$_3$Et$_2$)$_4^{3+}$ (see Figure 1) to compare the effects of chemical variation in amide substituents on the pH sensitivity of CEST from –NH exchange in these molecules. Our long-term goal is to identify mixtures of agents with highly shifted –NH protons that can be selectively activated even in the presence of a broad water signal typical of that seen *in vivo* for ratiometric imaging of tissue pH.

2. RESULTS AND DISCUSSION

High-resolution ^{1}H NMR spectra (not shown) of the three Yb(III) complexes showed typical hyperfine shifted resonances characteristic of other Yb(III) complexes of this type (11,13). The most easily assigned resonance is the most highly downfield-shifted macrocyclic axial proton, usually referred to as the H$_4$ resonance. This resonance appeared at 92 and 88 ppm in the NMR spectra of Yb-1 and Yb-2, respectively, and at 77 ppm in the spectrum of Yb-3. This result indicates that the two negatively charged ligand side-chains provide similar ligand fields for the Yb(III) ion while the phosphonate diethyl ester ligand (no charge) provides a considerably weaker ligand field (14). This same pattern was seen in chemical shift comparisons of the amide –NH protons. These were found near −17 ppm in NMR spectra of Yb-1 and Yb-2, and −13 ppm in the spectrum of Yb-3. Here again, the smallest chemical shift was observed for the uncharged DOTA–(NHCH$_2$PO$_3$Et$_2$)$_4$ ligand, consistent with a weaker ligand field.

Application of a frequency-selective, presaturation pulse on the –NH resonance in each of these samples results in a reduction in the bulk water signal, a characteristic CEST response that results from proton exchange between the –NH proton and bulk water. The magnitude of this CEST effect is, of course, pH- and temperature-dependent. Figure 2 shows the percentage decrease in water intensity, $[1 - (M_s/M_o)]$, as a function of pH for the three Yb(III) complexes. All three curves have a similar shape, with amide CEST increasing with pH up to a maximum value then decreasing with a further increase in pH. This behavior is characteristic of base-catalyzed –NH proton exchange which reaches an optimal exchange rate at the apex of the CEST vs pH curves for the three complexes, at pH 8.3 for Yb-1, pH 8.8 for Yb-2 and pH 6.9 for Yb-3. These differences in pH where maximum CEST occurs clearly reflect differences in amide proton exchange rates in the three molecules and likely also differences in their pK_as (unknown). The potentiometric titrations of DOTA–(gly)$_4$ (ligand 1) have been reported (15,16), but no high protonation steps attributable to amide protons were detected up to pH 11.7. Coordination of the amide oxygen to the Yb(III) results in sharing of the amide nitrogen lone pair electrons with the carbonyl carbon and this, in turn, increases the acidity of the amide proton and makes base-catalyzed proton exchange more efficient (17,18). The presence of an additional charged substituent near the amide nitrogen can either stabilize or destabilize this electron delocalization and thereby affect proton exchange as well (19). One would predict then that negatively charged substituents on the amide groups of Yb-1 and Yb-2 should make it more difficult to remove a proton from the amide and subsequently require a higher base concentration to initiate proton exchange. This is observed experimentally. The more highly charged substituent, -CH$_2$-PO$_3^{2-}$ (Yb-2) makes removal of the amide proton more difficult compared with the –CH$_2$-CO$_2^-$ substitutent (Yb-1) so the apex of its curve lies at more basic pH. Conversely, the uncharged substituent, -CH$_2$-PO(OEt)$_2$ (Yb-3) allows for easier proton removal as evidenced by the shift in the apex of the curve for Yb-3 to lower pH (Figure 2). These results demonstrate that it should be relatively easy to shift the amide CEST curve to almost any desired pH range by altering the structure of the amide substituent.

Theory also predicts that the optimal proton lifetime (τ_M) required to achieve maximal CEST depends upon the strength of the applied field (B_1) (see equation 2). Thus, for a B_1 of 900 Hz, the optimal residence lifetime of a proton should occur near 0.18 ms while for a B_1 of 300 Hz, the optimal lifetime would be longer, 0.53 ms. To test this experimentally, CEST vs pH profiles were recorded for Yb-1 and Yb-3 at four different applied B_1 values (Fig. 3). For both agents, it can be seen that the apexes of the
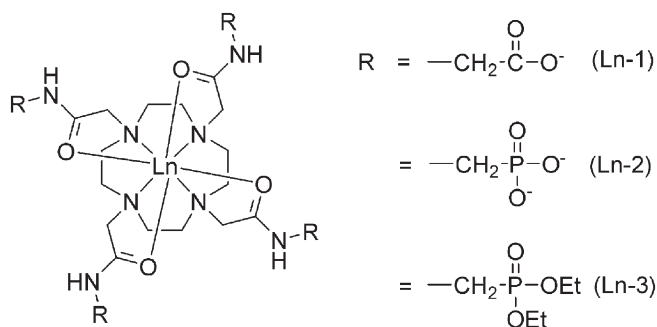
Figure 1. Molecular structures of the LnDOTA-tetraamide complexes investigated in this paper.
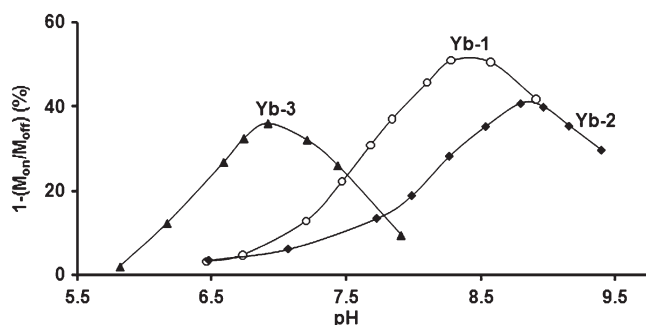
Figure 2. pH dependence of CEST intensity $[1 - (M_{on}/M_{off})]$ for Yb-1 (open circles), Yb-2 (solid diamonds) and Yb-3 (solid triangles) recorded on 20 mM samples at 9.4 T, 298 K ($B_1 = 500$ Hz, sat. time = 4 s).
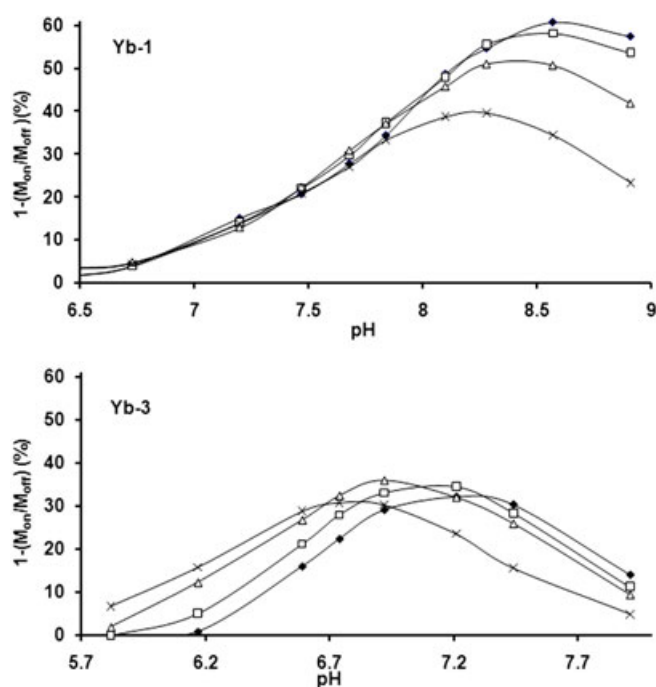
Figure 3. CEST vs pH profiles for Yb-1 (top) and Yb-3 (bottom) at different B_1, 900 Hz (solid diamonds), 700 Hz (open squares), 500 Hz (open triangles), 300 Hz (×) recorded on 20 mM solutions at 9.4 T, 298 K (sat. time = 4 s).

CEST vs pH curves vary with B_1 as predicted. Reasonable agreement (±0.1 ms) between the theoretical and experimental τ_{NH} values was observed for both agents at all four power levels. These data demonstrate that the shape and position of the CEST vs pH curves is determined by the applied B_1.

A more interesting and perhaps less obvious difference between the CEST vs pH curves for Yb-1 and Yb-3 is that CEST increases with B_1 (as expected) at or near the pH optima for Yb-1 but does not increase nearly as much with increasing B_1 for Yb-3. The reason for this apparent anomaly is that amide proton exchange rates are so much faster for Yb-3 than Yb-1 at all pH values. This is apparent from the observation that one must go to much lower pH values to slow down –NH proton exchange enough for CEST to disappear for Yb-3 than for Yb-1. In comparison, the –NH exchange lifetime for Yb-3 at pH 7.5 is 0.11 ms while the –NH exchange lifetime for Yb-1 at this same pH is 3.3 ms, a 30-fold difference in exchange rates. Given that proton exchange is faster for Yb-3 at any given pH value, this leads to more rapid convergence of the exchanging –NH proton resonance with the bulk water resonance with an applied field, B_1. Hence, the CEST vs pH curves for Yb-1 continue to increase with B_1 near the optimal pH region while CEST for Yb-3 reaches a near plateau with increasing B_1.

There is great interest in developing MRI sensors for mapping whole body tissue pH to distinguish normal from diseased tissues. In particular, images that report the extracellular pH of tumors would be of great diagnostic value (20). A CEST vs pH curve that covers a range of pH values from 7.4 to below 6 would be ideal for this purpose. While the CEST curves for Yb-1 and Yb-2 lie somewhat too far toward basic pH (Fig. 2), Yb-3 has an effective pH range between 6 and 7, depending upon applied B_1 (Fig. 3). Nevertheless, one would not be able to distinguish between a tissue pH above 7.4 vs one below about

pH 6.6 so using Yb-3 alone would not be optimal. One way of overcoming this limitation is by combining Yb-3 with another agent that has a different chemical shift and is more sensitive to changes in pH over a more basic pH range, such as Yb-1 or Yb-2. Yb-1 was chosen for further experimentation because of its steeper CEST vs pH curve (Fig. 2). Combining Yb-1 and Yb-3 together should not only increase the effective pH range but it also offers the possibility of ratiometric imaging to obtain a concentration-independent measure of pH (9).

The relatively small chemical shift dispersion of the amide protons in these Yb(III) complexes compared with the bulk water signal would be even more problematical *in vivo* because of the underlying magnetization transfer (MT) signal arising from water tightly associated with proteins and other large macromolecules (17,21,22). One solution might be to shift the amide proton resonance frequencies even further away from the bulk water signal by choosing a different lanthanide ion. Tm(III) is perhaps the best choice for this purpose as this paramagnetic ion is known to induce much larger chemical shifts in all ligand protons compared to Yb(III) without introducing too much line broadening (11). For comparison, the chemical shifts of the –NH protons in the ^{1}H NMR spectra of Tm-1 and Tm-3 are at –51 and –40 ppm, respectively, about 3-fold larger than the shifts in the corresponding Yb(III) complexes.

CEST vs pH curves were collected for solutions of Tm-1 and Tm-3 at 310 K (Fig. 4). Although the general shapes of these curves were qualitatively similar to the corresponding Yb-1 and Yb-3 complexes (compare Figs 2 and 4), the maximum in the CEST vs pH curve for Tm-1 is shifted slightly toward lower pH while the maximum in the curve for Tm-3 is shifted toward higher pH. The fact that these two compounds differ in their pH sensitivity suggests that one should be able to use a mixture of the two complexes and ratiometric imaging to obtain a concentration independent measure of pH. To examine this possibility, CEST spectra of equimolar mixture of Tm-1 and Tm-3 as a function of pH are shown in Fig. 5. Again, the general shapes of the CEST vs pH curves for each individual agent were similar to those shown for separate agents in Fig. 4 but the total CEST intensities of the mixture was somewhat smaller than that observed in the single agent samples because the higher total concentration of Tm(III) (40 mM) shortened the T_1 of the bulk solvent protons. In this case, the T_1 of bulk water for 20 mM solutions of Tm-1 or Tm-3 at 310 K averaged about 0.5 s while the T_1 of water containing the mixture (total Tm = 40 mM) was 0.25 s.

A ratiometric analysis described previously by Ward and Balaban for diamagnetic molecules was used to obtain a
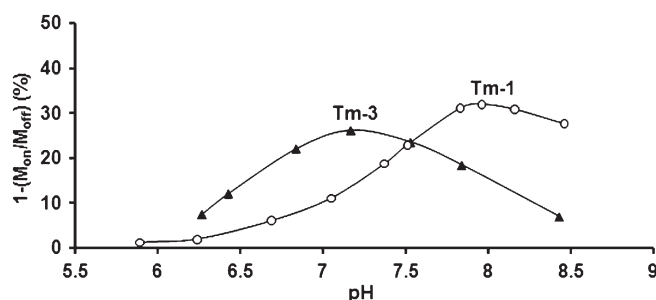
Figure 4. CEST vs pH profiles for separate 20 mM samples of Tm-1 (open circles) and Tm-3 (solid squares) recorded at 9.4 T and 310 K (B_1 = 500 Hz, sat. time = 4 s).
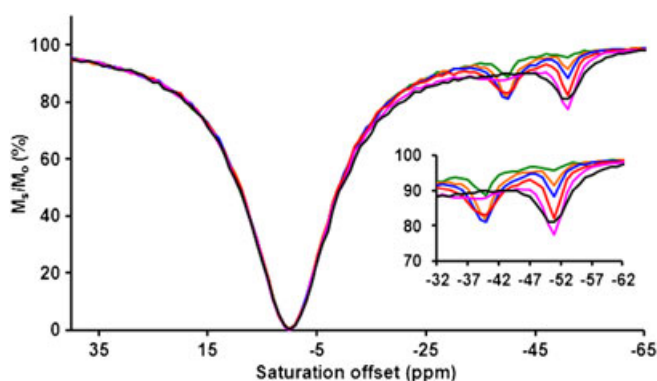
Figure 5. CEST profile of 20 mM Tm-1 and 20 mM Tm-3 in a single solution at different pH values (green = pH 6.4, orange = pH 7.0, blue = pH 7.3, red = pH 7.5, pink = pH 8.1, black = pH 8.3) recorded at 9.4 T and 310 K ($B_1 = 500$ Hz, sat. time = 4 s). The inset provides a close-up view of the amide proton CEST peaks.

Figure 6. Ratiometric plots for an equimolar mixture of Tm-1 and Tm-3 (20 mM each) recorded at 400 MHz and 310 K ($B_1 = 500$ Hz, sat. time = 4 s).

concentration-independent measure of pH (9). Here, the ratios of CEST from the two unique chemical exchange sites (sites 1 and 2) were measured and plotted as follows.

$$\frac{\left(\frac{(M_o - M_s)^{Site1}}{M_s^{Site1}}\right)}{\left(\frac{(M_o - M_s)^{Site2}}{M_s^{Site2}}\right)} = \frac{k_{ex}^{Site1}[Agent]^{Site1}n^{Site1}}{k_{ex}^{Site2}[Agent]^{Site2}n^{Site2}} \quad (3)$$

Equation (3) illustrates that the CEST ratio, $[(M_o - M_s)^{Site1}/M_s^{Site1}]/[(M_o - M_s)^{Site2}/M_s^{Site2}]$, is proportional to the ratio of the agent concentrations, the number of exchangeable protons at each site (4 in this case), and the proton exchange rates at the two sites, k_{ex}. This equation also assumes that both exchange sites are fully saturated after application of a long presaturation pulse. Since both rates are pH dependent, a plot of the CEST ratio as a function of pH yields a standard curve that is independent of [Agent] and n. This is important because the local concentration of the agent in tissue is unknown in most cases and this is usually required for most pH measurements *in vivo*. Such ratiometric CEST measurements on other paramagnetic systems have been shown to provide a concentration-independent measure of pH by several authors (9,11,12,23,24) and, more recently, Wu *et al.* (25).

The ratiometric curve reported in Fig. 6 was generated by collecting two CEST spectra and taking the ratio of water intensities, Tm-3 (pre-saturation at −40 ppm)/Tm-1 (pre-saturation at −51 ppm) as a function of solution pH. The resulting ratiometric plot covers a broader pH range (pH 6.4–7.4) than seen previously for any of the individual agents. This extended pH range could prove important in imaging the extracellular pH of individual tumors or in differentiating between infarcted or poorly perfused tissues from well-perfused tissues using CEST-MRI. Of course, calibration curves such as the one shown in Fig. 6 will depend on factors such as B_1, field strength, and concentration so separate calibration curves should be generated for each particular experimental protocol. Although we do not demonstrate here that this ratiometric plot is indeed independent of agent concentration as theory predicts, we have shown recently that this same ratiometric method works well for a pH-dependent PARACEST agent over a wide concentration range (25).
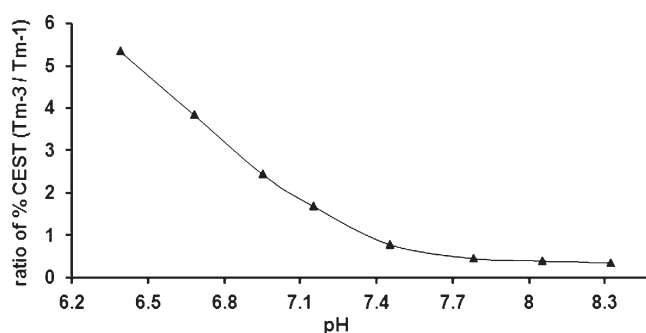
For practical applications, Tm-1 and Tm-3 cannot be assumed to distribute identically in tissues owing to the differences in their charge and molecular size. This limitation could potentially be overcome by encapsulating both the agents in a single nano-carrier such as a liposome. A liposome filled with two types of Tm(III) CEST agents would not only insure that an identical amount of each agent would occupy the same tissue space, but such a system could potentially increase the CEST sensitivity of such a pH sensor by increasing the local agent concentration at the site of interest. Of course, proton exchange rates may also be slower due to the additional liposomal bilayer barrier so this may be a trade-off. The approach taken here using two Tm(III) complexes also has some potential advantages over the pH-sensitive YbDOTAM dendrimers reported previously (24), especially for ratiometric imaging. The two Tm(III) complexes studied here have the advantage of having a larger chemical shift difference between the two amide protons compared with the different Yb(III) dendrimers and the –NH exchange sites in the Tm(III) complexes are shifted further away from the bulk water frequency so the potential interference with the tissue MT signal is further minimized.

3. CONCLUSIONS

Three lanthanide-based PARACEST agents bearing different charges on the amide substituent were reported in this study. The differences in the electrostatic properties of the appended amide group altered both the –NH exchange rates and resonance frequencies of the amide protons. Consequently, this affects the pH sensitivity range of the amide proton saturation transfer to bulk water. It was shown that a shift in the apex of a CEST vs pH curve correlated with the ability of the substituent to stabilize the negative charge on the deprotonated form of the amide. A most highly negative substituent ($-CH_2-PO_3^{2-}$) destabilized this charge and this resulted in a shift in the apex to a more basic pH value (pH 8.8) while the neutral amide substituent [$-CH_2-PO(OEt)_2$] shifted the apex of the CEST vs pH curve toward a lower pH value (pH 6.9). These observations led to further studies of agent mixtures, each having a different amide proton chemical shift and pH-responsive regions to create a pH sensor that covers a broader pH range required for many clinical applications. This study could provide an avenue to further explore the potential of amide proton exchange by fine-tuning the properties of the amide side-arm.

4. EXPERIMENTAL

The synthesis of DOTA–$(NHCH_2PO_3Et_2)_4$, DOTA–$(NHCH_2PO_3)_4{}^{8-}$ and DOTA–$(gly)_4{}^{4-}$ was performed using a previously reported method (11,13,26).

4.1. NMR spectroscopy

NMR samples for CEST studies were prepared by dissolving an agent in H_2O (400 µL) at a concentration of 100 mM. The pH was adjusted by addition of either lithium hydroxide monohydrate or p-toluenesulfonic acid monohydrate to avoid dilution.

4.2. CEST measurements

All CEST spectra were recorded on a Bruker Avance III 400 spectrometer at 298 K (for Yb complexes) and 310 K (for Tm complexes) by application of a 4 s frequency-selective presaturation pulse over a range of frequencies followed by a single observe pulse to measure the residual water signal. Two signal averages were collected at each presaturation frequency. Prior to collection of the full CEST spectra, single frequency CEST intensity measurements showed that 4 seconds was sufficient to reach full saturation of each exchanging –NH proton. The bulk water signal intensity, M_s/M_o, is plotted as a function of saturation frequency and is referred to as the Z-spectrum or, recently, the CEST spectrum. In this experiment, the sample was irradiated with four different presaturation pulses (B_1, 21.2, 16.5, 11.8 or 7.0 µT) at a 4 s duration over the range of ±100 ppm saturation frequencies (saturation offset). The CEST effect was determined by taking the bulk water signal intensity from the CEST spectrum at the resonance frequency of the exchanging proton (on-resonance) and at the same offset frequency but on the opposite side with respect to the bulk water signal intensity (off-resonance). The bulk water signal was set to 0 ppm. This method takes into account the direct saturation effects of the bulk water signal.

4.3. Fitting CEST spectra to the Bloch equations modified for exchange

The resulting CEST spectra were fitted to the Bloch equations for a three-site exchange pool model (bulk water, water coordinated with the Ln(III), and the amide proton) using a MATLAB™ program (27). The T_1 of the bulk water proton was measured using the inversion recovery method using a Bruker Avance spectrometer operating at 400.13 MHz, while T_2 was estimated by taking the full width at half height of the bulk water proton peak. The following parameters were also included in the fitting program: presaturation pulse (B_1) in Hz, magnetic field (B_0), presaturation time, T_1 and T_2 of bulk water, and proton concentrations and resonance frequencies of bulk water, bound water and amide. The residence lifetime (τ_M) of the amide protons was determined by averaging the fits of several CEST spectra collected using at least four different B_1 values (900, 700, 500, 300 Hz or 21.2, 16.5, 11.8 or 7.0 µT, respectively) and subsequently converted to amide proton exchange rates ($k_{ex} = 1/t_M$).

Acknowledgments

REFERENCES

1. Forsen S, Hoffman RA. Study of moderately rapid chemical exchange reactions by means of nuclear magnetic double resonance. J Chem Phys 1963; 39: 2892–2901.
2. Wolff SD, Balaban RS. Magnetization transfer contrast (MTC) and tissue water proton relaxation in vivo. Magn Reson Med 1989; 10: 135–144.
3. Zhou JY, van Zijl PCM. Chemical exchange saturation transfer imaging and spectroscopy. Prog Nucl Magn Reson Spectrosc 2006; 48: 109–136.
4. Aime S, Barge A, Botta M, De Sousa AS, Parker D. Direct MMR spectroscopic observation of a lanthanide-coordinated water molecule whose exchange rate is dependent on the conformation of the complexes. Angew Chem Int Edn 1998; 37: 2673–2675.
5. Zhang SR, Winter P, Wu KC, Sherry AD. A novel europium(III)-based MRI contrast agent. J Am Chem Soc 2001; 123: 1517–1518.
6. Aime S, Delli Castelli D, Terreno E. Novel pH-reporter MRI contrast agents. Angew Chem Int Ed 2002; 41: 4334–4336.
7. Zhang SR, Merritt M, Woessner DE, Lenkinski RE, Sherry AD. PARACEST agents: modulating MRI contrast via water proton exchange. Acc Chem Res 2003; 36: 783–790.
8. Woods M, Donald EWC, Sherry AD. Paramagnetic lanthanide complexes as PARACEST agents for medical imaging. Chem Soc Rev 2006; 35: 500–511.
9. Ward KM, Balaban RS. Determination of pH using water protons and chemical exchange dependent saturation transfer (CEST). Magn Reson Med 2000; 44: 799–802.
10. Guivel-Scharen V, Sinnwell T, Wolff SD, Balaban RS. Detection of proton chemical exchange between metabolites and water in biological tissues. J Magn Reson 1998; 133: 36–45.
11. Aime S, Barge A, Castelli DD, Fedeli F, Mortillaro A, Nielsen FU, Terreno E. Paramagnetic lanthanide(III) complexes as pH-sensitive chemical exchange saturation transfer (CEST) contrast agents for MRI applications. Magn Reson Med 2002; 47: 639–648.
12. Terreno E, Castelli DD, Cravotto G, Milone L, Aime S. Ln(III)-DOTAMGly complexes: s versatile series to assess the determinants of the efficacy of paramagnetic chemical exchange saturation transfer agents for magnetic resonance imaging applications. Invest Radiol 2004; 39: 235–243.
13. Kalman FK, Woods M, Caravan P, Jurek P, Spiller M, Tircso G, Kiraly R, Brucher E, Sherry AD. Potentiometric and relaxometric properties of a gadolinium-based MRI contrast agent for sensing tissue pH. Inorg Chem 2007; 46: 5260–5270.
14. Dickins RS, Parker D, Bruce JI, Tozer DJ. Correlation of optical and NMR spectral information with coordination variation for axially symmetric macrocyclic Eu(III) and Yb(III) complexes: axial donor polarisability determines ligand field and cation donor preference. Dalton Trans 2003: 1264–1271.
15. Baranyai Z, Banyai I, Brucher E, Kiraly R, Terreno E. Kinetics of the formation of [Ln(DOTAM)](3+) complexes. Eur J Inorg Chem 2007: 3639–3645.
16. Baranyai Z, Brucher E, Ivanyi T, Kiraly R, Lazar I, Zekany L. Complexation properties of N,N′,N″,N‴-[1,4,7,10-tetraazacyclododecane-1,4,7,10-tetrayltetrakis(1-oxoethane-2,1-diyl)]tetrakis[glycine] (H(4)dotagl). Equilibrium, kinetic, and relaxation behavior of the lanthanide(III) complexes. Helv Chim Acta 2005; 88: 604–617.
17. Liepinsh E, Otting G. Proton exchange rates from amino acid side chains – implications for image contrast. Magn Reson Med 1996; 35: 30–42.
18. Englande SW, Downer NW, Teitelba H. Hydrogen-exchange. Annu Rev Biochem 1972; 41: 903–924.
19. Sheinblatt M. Nuclear magnetic resonance study of protolysis kinetics of peptide hydrogens of triglycine. J Am Chem Soc 1966; 88: 2123–2126.
20. Gatenby RA, Gawlinski ET, Gmitro AF, Kaylor B, Gillies RJ. Acid-mediated tumor invasion: a multidisciplinary study. Cancer Res 2006; 66: 5216–5223.
21. Henkelman RM, Stanisz GJ, Graham SJ. Magnetization transfer in MRI: a review. NMR Biomed 2001; 14: 57–64.
22. Eng J, Ceckler TL, Balaban RS. Quantitative H-1 magnetization transfer imaging in vivo. Magn Reson Med 1991; 17: 304–314.
23. Ali MM, Yoo B, Pagel MD. Tracking the relative in vivo pharmacokinetics of nanoparticles with PARACEST MRI. Mol Pharm 2009; 6: 1409–1416.

24. Pikkemaat JA, Wegh RT, Lamerichs R, van de Molengraaf RA, Langereis S, Burdinski D, Raymond AYF, Janssen HM, de Waal BFM, Willard NP, Meijer EW, Grull H. Dendritic PARACEST contrast agents for magnetic resonance imaging. Contrast Media Mol Imag 2007; 2: 229–239.
25. Wu YK, Soesbe TC, Kiefer GE, Zhao PY, Sherry AD. A responsive europium(III) chelate that provides a direct readout of pH by MRI. J Am Chem Soc 2010; 132: 14002–14003.
26. Ali MM, Woods M, Caravan P, Opina ACL, Spiller M, Fettinger JC, Sherry AD. Synthesis and relaxometric studies of a dendrimer-based pH-responsive MRI contrast agent. Chem Eur J 2008; 14: 7250–7258.
27. Woessner DE, Zhang SR, Merritt ME, Sherry AD. Numerical solution of the Bloch equations provides insights into the optimum design of PARACEST agents for MRI. Magn Reson Med 2005; 53: 790–799.